Tunable terahertz amplification in optically excited biased semiconductor superlattices: Influence of excited excitonic states

Dawei Wang,[1] Aizhen Zhang,[1] Lijun Yang,[2] and Marc M. Dignam[1]
[1]*Department of Physics, Queen's University, Kingston, Ontario, Canada K7L 3N6*
[2]*Chemistry Department, University of California, Irvine, California 92697-2025, USA*
(Received 2 November 2007; revised manuscript received 10 January 2008; published 7 March 2008)

We simulate the coherent carrier dynamics of an optically excited, undoped AlGaAs superlattice in the presence of a terahertz pulse using an excitonic formalism that includes 1*s* excitonic states as well as higher in-plane excited states and allows for dephasing and population decay. We show that this system exhibits tunable terahertz gain due to excitonic effects, even in the presence of a large number of unbound excitons. We find that gain coefficients greater than 20 cm^{-1} can be achieved over a tuning range of 3–11 THz and that due to the *coherent* cascading of the carriers down the excitonic Wannier-Stark ladder, the gain coefficients have much higher gain saturation fields than comparable two-level systems.

DOI: 10.1103/PhysRevB.77.115307 PACS number(s): 73.21.Cd, 42.65.Yj, 78.47.−p, 78.67.Pt

I. INTRODUCTION

The development of a compact, tunable terahertz (THz) laser has been an area of intense research for over a decade. One of the first THz lasers was the quantum cascade laser (QCL). First demonstrated in 1994 (Ref. 1) at infrared frequencies, QCLs are now available in the few THz range.[2–4] They employ a periodic array of *doped* multiquantum wells and use intersubband electron transitions to generate THz radiation. Phonon-assisted carrier cascading is employed to depopulate lower lasing levels and repopulate upper lasing levels further down the structure, thus maintaining population inversion and allowing one electron to produce many THz photons. Although the QCL is a *compact* THz source, it only has very limited tunability ($\sim \pm 4\%$) (Refs. 5 and 6) due to the fact that the gain spectrum of a QCL is largely fixed by its structure.

In this work, we demonstrate the possibility of *tunable* THz gain in an *undoped,* optically excited, biased semiconductor superlattice (BSSL). The gain mechanism arises from transitions between the different *excitonic* Wannier-Stark ladder (WSL) states, tunability is provided by the applied dc bias, and depopulation of lower lasing levels is provided via *coherent cascading* of excitons down the excitonic WSL. By performing detailed quantum-coherent simulations for bias fields ranging from 15 to 60 kV/cm, we show that our BSSL has THz gain coefficients comparable to those obtained in QCLs ($\sim$20 cm^{-1}) but tunable over a frequency range of 3–11 THz.

It is well known that under a spatially constant electric field F_o, the degeneracy of electronic energy levels of a superlattice is generally broken, giving rise to localized electronic eigenstates known as the WSL.[7] In the single-electron picture, the electronic states of a BSSL form the WSL with energies $E_n = E_0 + n\hbar\omega_B$, where n is an integer and $\omega_B = eF_o d/\hbar$ is the Bloch oscillation (BO) frequency and d is the periodicity of the superlattice. For BSSLs with periodicity of several nanometers, the energy difference between these levels is a few THz at moderate fields ($\sim$10 kV/cm) and is tunable with F_o. Because the energy levels are equally spaced and the transition dipole matrix elements are the same for the n to $(n+1)$ and n to $(n-1)$ transitions, it has been shown in the single-electron picture that although a THz field will induce transitions between the WSL levels associated with a given band, because the levels are equally spaced, such a system cannot provide gain for THz radiation due to the absorption-emission symmetry.[8] It has been proposed that phonon-assisted transitions will break the symmetry so as to favor gain when $\nu < \nu_B$.[9] However, this gain is expected to be rather weak as it is a second-order process[10] and has not yet been conclusively demonstrated.

Beyond the single-particle approximation, the electron WSL states are not eigenstates of a BSSL. As has been shown previously,[11] when Coulomb interaction is considered, an excitonic WSL is formed from 1*s*-like excitonic states that has *unequal energy spacings* and unequal intraband dipole moments between neighboring WSL states.[11,12] Except at very low bias fields, these 1*s* excitonic levels can still be labeled by the WSL index n, such that the along-axis electron-hole separation is approximately nd and the intraband dipole moment of the state is approximately $-nde$. The unequal spacing in the 1*s* excitonic WSL is due to the fact that 1*s* states with smaller $|n|$ have larger binding energies arising from the smaller electron-hole separation. This unequal spacing, along with an attendant asymmetry in the intraband transition dipoles, results in the breaking of the absorption-emission symmetry and so gain is now possible. Unlike the phonon-assisted asymmetry,[9] this excitonic asymmetry is a first-order process which by itself can produce very large gain coefficients. This mechanism for gain in an optically pumped undoped BSSL was first proposed by Lachaine *et al.*[12] and was investigated for THz pulses by Zhang *et al.*[13] In this previous work, however, we did not investigate the dependence of the gain on bias or on the THz field amplitude. Most importantly, in that work, the calculations were performed employing only 1*s* exciton states.

Although 1*s* states dominate the optical response of a BSSL when the exciting pulse is centered below the $n=0$ 1*s* excitonic WSL state, higher in-plane excited states (HIESs) have been shown to be important in obtaining accurate results at moderate bias fields and higher optical frequencies.[14,15] Because of the large binding energies of the

1*s* states, the 1*s* WSL has a much greater asymmetry than the WSLs associated with HIES, and so most of the net gain arises from transitions within the 1*s* WSL. In fact, we find that generally, the maximum gain can be achieved when the optical excitation is resonant with the $n=0$ 1*s* heavy-hole exciton. With such an excitation frequency, many HIESs are generally created. To model this system under these conditions, it is important to include the HIES. Thus, in this work, we examine the effect of the HIES on the THz gain coefficients and gain saturation characteristics of the system. We find that for a given optical pulse intensity, the inclusion of HIES reduces the THz gain coefficient, but the reduction is less than a factor of 2 for a wide range of bias fields. We also show that the gain saturation of our BSSL is much better than that for a two-level system.

The paper is organized as follows. In Sec. II, we present our excitonic approach in calculating intraband polarization and equations for calculating THz gain coefficients. In Sec. III, we present the calculated THz gain spectra for a range of bias fields and investigate the influence of HIES on the gain. In Sec. IV, we discuss the coherent cascading properties of the BSSL and its effects on gain saturation. Finally, in Sec. V, we present our conclusions.

II. THEORY

In this section, we introduce our excitonic approach in calculating THz gain coefficients. Some of the equations presented below have been derived and used in previous publications;[12,15–17] we include the central equations here to aid in the discussion of the results and approach used. We first describe the excitonic Wannier-Stark ladder that arises due to Coulomb interactions between electrons and holes. We then show how the intraband polarization $\langle P_{\text{intra}}(t)\rangle$ can be obtained by calculating excitonic correlation functions $\langle B_\mu^\dagger B_\nu\rangle$. Finally, equations used to calculate gain coefficients from $\langle P_{\text{intra}}(t)\rangle$ are given.

A. Our model and excitonic Wannier-Stark ladder

The system we consider is the $GaAs/Ga_{0.7}Al_{0.3}As$ superlattice (SL) with a 67 Å well and a 17 Å barrier that has been previously investigated both experimentally and theoretically.[12,15,18,19] A bias is applied along the growth axis to produce a uniform dc field F_o that splits the electron and hole minibands of the SL into localized eigenstates that form the WSL.[7] If the electron-hole Coulomb interaction is neglected, the energy levels are equally spaced and for our BSSL with $F_o=15$ kV/cm, $\hbar\omega_B=12.6$ meV, corresponding to a Bloch frequency of $\nu_B=\omega_B/2\pi=3.0$ THz.

In our excitonic approach, we treat the heavy-hole excitons as the fundamental excitations in a BSSL, as they are the lowest excited states and dominate the THz response for the excitation condition considered in this paper. Thus, to derive our dynamic equations for the polarization, we first have to calculate and describe the excitonic states of the BSSL. Based on the work of Dignam and Sipe,[20] the exciton states for various BSSLs have been calculated and compared successfully with experiment via absorption spectra.[15] The

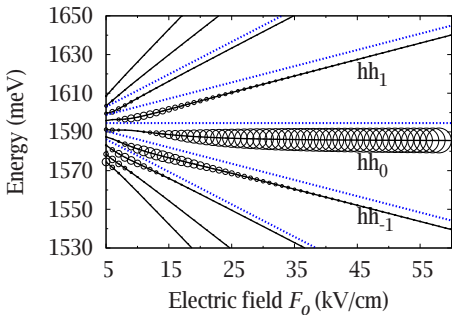

FIG. 1. (Color online) The WSL fan diagram for the 1*s* heavy-hole excitons (solid line) and noninteracting electron-hole pairs (blue dotted line). The diameter of the open circles for the 1*s* WSL levels is proportional to the optical oscillator strength.

calculations are based on the expansion of the BSSL excitonic states in terms of the so-called two-well (TW) excitonic states, which have electrons and holes in wells separated by *pd*, where $p=-N/2,\ldots,N/2$.[20,21] In earlier work,[21,20] these basis excitonic states were simply 1*s*-like states in the plane; in later calculations, these states include many HIESs, up to and including continuum states.[15,19] In such calculations, we can choose how many two-well exciton states are used. In our previous work on THz gain in BSSLs,[12,13,17] we employed only the 1*s* states. In this paper, we present calculations with $N=12$ and with 60 TW excitonic states for each TW separation: the 1*s* state plus 59 additional higher in-plane excited excitonic WSL states of *s* symmetry (*full basis*). We find that this number of states is sufficient for convergence for the calculations presented. To make the effects of the HIES clear, in the following sections, we also present results of calculations that using a basis includes only the 1*s* excitons (1*s basis*).

In Fig. 1, we plot the calculated energy levels $\hbar\omega_n$ of the 1*s* heavy-hole exciton WSL as a function of F_o along with the levels found neglecting the excitonic effect. The different levels are labeled by the WSL index *n* such that the along-axis electron-hole separation is approximately *nd* and the intraband dipole moment of the state is approximately $-nde$. From this figure, it is clear that the unequal spacing in the 1*s* excitonic WSL levels is due to the fact that 1*s* states with smaller $|n|$ have larger binding energies arising from the smaller electron-hole separation.

Table I shows frequency difference between the 1*s* excitonic WSL states; in contrast to the ideal WSL, it is clear that the spacings in the 1*s* excitonic WSL are not equal. For example, for $F_o=15$ kV, the energy difference between $n=0$ and -1 states is given by $\omega_0-\omega_{-1}=0.9555\omega_B$ while $\omega_1-\omega_0=1.0412\omega_B$. As the absorption-emission symmetry is broken, we expect that net gain or loss will be possible, depending on the frequency of the incident THz field and the optical excitation conditions of the BSSL.

In Fig. 2, we present the calculated linear optical absorption spectra for the BSSL for (a) $F_o=15$ kV/cm and (b) $F_o=60$ kV/cm using two different bases, the 1*s* basis and the full basis. For the 1*s* basis, the peaks are associated with individual 1*s* heavy-hole excitonic WSL states hh_n with energy $\hbar\omega_n$. For $F_o=15$ kV/cm, when we use the full basis, the

TABLE I. Frequency difference between excitonic Wannier-Stark ladder states for F_o=15, 30, and 60 kV/cm.

Frequency difference	F_o=15kV/cm (ω_B)	F_o=30kV/cm (ω_B)	F_o=60kV/cm (ω_B)
$\omega_{-3}-\omega_{-4}$	0.9741	0.9828	0.9912
$\omega_{-2}-\omega_{-3}$	0.9167	0.9685	0.9849
$\omega_{-1}-\omega_{-2}$	0.8420	0.9250	0.9654
$\omega_{0}-\omega_{-1}$	0.9555	0.8686	0.9157
$\omega_{1}-\omega_{0}$	1.0412	1.1245	1.0812
$\omega_{2}-\omega_{1}$	1.1474	1.0744	1.0355
$\omega_{3}-\omega_{2}$	1.0870	1.0360	1.0165
$\omega_{4}-\omega_{3}$	1.0494	1.0196	1.0092

HIESs result in a broadening of the peaks and the inclusion of the steplike continuum absorption spectrum. The steps are due to the creation of carriers in the HIES WSLs. As a result, even if we excite on resonance with, say, the n=0 1s WSL state, we also excite a large number of HIES with lower WSL indices. We note that there is some mixing of the 1s states with the resonant HIESs that have a lower WSL ladder index; this leads to effects such as Fano resonances. For simplicity of discussion, however, we shall refer to the states simply as 1s states or HIES and assign them a definite WSL index; this has been shown to be a good qualitative description for the BSSL and dc fields considered here.[15] The absorption spectrum obtained for F_o=60 kV/cm is similar. However, for such high fields, due to the high degree of Wannier-Stark localization, only the n=0 1s exciton has an appreciable oscillator strength and state mixing is much less.

B. Hamiltonian and excitonic dynamic equations

An excitonic basis approach has been developed to calculate carrier dynamics in BSSLs.[15,16,22,23] In this approach, the Hamiltonian for a photoexcited BSSL is given by

$$H = H_{\text{ex}} + H_{\text{ex-opt}} + H_{\text{ex-THz}}, \tag{1}$$

where

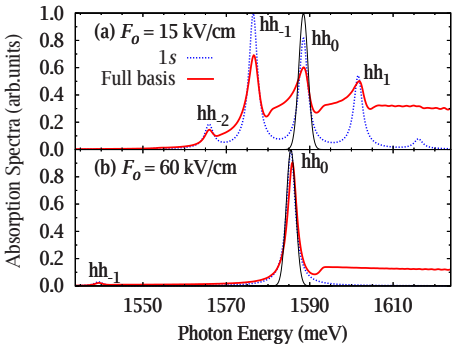

FIG. 2. (Color online) Optical absorption spectrum calculated for the BSSL for (a) F_o=15 kV/cm and (b) F_o=60 kV/cm. The solid (red) lines are calculated using the full basis, while the dashed (blue) lines are calculated employing only 1s states. The thin black lines indicate the power spectrum of the exciting optical pulse.

$$H_{\text{ex}} = \sum_{\mu} E_{\mu} B_{\mu}^{\dagger} B_{\mu} \tag{2}$$

is the Hamiltonian for the noninteracting superlattice excitons in the presence of the external dc electric field F_o. $B_{\mu}^{\dagger}$ (B_{μ}) is the creation (annihilation) operator for an exciton with internal quantum number μ and energy E_{μ}. $H_{\text{ex-opt}}$ describes the interaction between the excitation optical field $E_{\text{opt}}(t)$ and the excitons,

$$H_{\text{ex-opt}} = -V\boldsymbol{E}_{\text{opt}}(t) \cdot \boldsymbol{P}_{\text{inter}}, \tag{3}$$

where V is the volume of the system and $\boldsymbol{P}_{\text{inter}}$ is the interband polarization operator defined by

$$\boldsymbol{P}_{\text{inter}} = \frac{1}{V}\sum_{\mu} (\boldsymbol{M}_{\mu} B_{\mu}^{\dagger} + \boldsymbol{M}_{\mu}^{*} B_{\mu}). \tag{4}$$

In Eq. (4), $\boldsymbol{M}_{\mu}$ is the interband dipole matrix element of the μth excitonic state that can be obtained using exciton envelop functions. The last term in the Hamiltonian is the interaction term between the THz field and the excitons, which is given by

$$H_{\text{ex-THz}} = -V\boldsymbol{E}_{\text{THz}}(t) \cdot \boldsymbol{P}_{\text{intra}}, \tag{5}$$

where

$$\boldsymbol{P}_{\text{intra}} = \frac{1}{V}\sum_{\mu,\mu'} \boldsymbol{G}_{\mu\mu'} B_{\mu}^{\dagger} B_{\mu'} \tag{6}$$

is the intraband polarization of the BSSL system and $\boldsymbol{G}_{\mu\nu}$ is the intraband dipole matrix element between two excitonic states $|\psi^{\mu}\rangle$ and $|\psi^{\nu}\rangle$, given by

$$\boldsymbol{G}_{\mu\nu} = \langle \psi^{\mu} | -e(\boldsymbol{r}_e - \boldsymbol{r}_h) | \psi^{\nu} \rangle. \tag{7}$$

The derivations of the general forms of the interband, the intraband dipole matrix elements, and exciton dipole-dipole interaction that gives rise to $H_{\text{ex-ex}}$ are given in Ref. 22. We note that the above Hamiltonian does not include many-body effects such as exciton-exciton interactions, dynamic screening, or phase-space filling. In a number of recent papers, we have examined such effects.[15,19,22,23] These effects manifest themselves as a nonlinear optical response, which, in turn, modifies the THz response of the system. The effects of exciton-exciton interactions on the THz gain were calculated in Ref. 13. As such effects are at least fourth order in the optical field, for simplicity, we ignore them and consider only optical intensities that are low enough such that these effects can be ignored. Ultimately, these effects will likely limit the allowable carrier density and thus the maximum gain coefficient possible.

Using the Hamiltonian of Eq. (1) and the Heisenberg equation of motion, we obtain the dynamic equations for the interband and intraband correlation functions. The dynamic equation for $\langle B_{\mu}^{\dagger} \rangle$ is obtained by truncating to the first order of optical field,[12]

$$i\hbar\frac{d}{dt}\langle B_\mu^\dagger\rangle = \left(E_\mu - \frac{i\hbar}{T_{2\text{inter}}}\right)\langle B_\mu^\dagger\rangle + \boldsymbol{E}_{\text{opt}}(t)\cdot\boldsymbol{M}_\mu + \boldsymbol{E}_{\text{THz}}(t)\cdot\sum_\nu \boldsymbol{G}_{\mu,\nu}\langle B_\nu^\dagger\rangle. \quad (8)$$

To second order of the optical field, the intraband correlation function $\langle B_\mu^\dagger B_\nu\rangle$ is given by

$$i\hbar\frac{d}{dt}\langle B_\mu^\dagger B_\nu\rangle = -\left(E_\nu - E_\mu + \frac{i\hbar}{T_{\mu\nu}}\right)\langle B_\mu^\dagger B_\nu\rangle + \boldsymbol{E}_{\text{opt}}(t)\cdot[\boldsymbol{M}_\mu^*\langle B_\nu\rangle - \boldsymbol{M}_\nu\langle B_\mu^\dagger\rangle] + \boldsymbol{E}_{\text{THz}}(t)\cdot\sum_\gamma[\boldsymbol{G}_{\mu,\gamma}^*\langle B_\gamma^\dagger B_\nu\rangle - \boldsymbol{G}_{\nu\gamma}\langle B_\mu^\dagger B_\gamma\rangle]. \quad (9)$$

In these dynamic equations, interband, intraband dephasing time, and excitonic population decay are treated phenomenologically through time constants. In Eq. (8), $T_{2\text{inter}}$ is the interband dephasing time constant. In Eq. (9), $T_{\mu\nu}$ is an excitonic population decay time T_1 if $\mu=\nu$ and is an intraband dephasing time $T_{2\text{intra}}$ if $\mu\neq\nu$. The separation of intraband dephasing time and population decay time constants offers us extra flexibility in modeling real experiments; such a separation is not possible if one uses an electron-hole basis.[24] In our previous work,[13,17] we modeled exciton dephasing by including exciton-LO-phonon scattering explicitly. This was possible because we only employed a 1*s* basis. It is not feasible to use the same approach in the present case where we include many HIESs. However, in that work, we found no appreciable difference between results obtained including phonons and those obtained using phenomenological scattering time constants for pulsed THz fields as long as the various time constants chosen are appropriate and the THz pulse is not much longer than the intraband scattering time.

C. Obtaining terahertz gain coefficients

Since the intraband polarization of a BSSL acts as the source term in Maxwell's equations that gives rise to THz emission, THz gain spectra can be obtained by Fourier transforming temporal evolution of intraband polarization in the presence of an external THz pulse. The intraband polarization can be calculated numerically using the excitonic dynamic equations of Eqs. (8) and (9) shown in Sec. II B.

After the BSSL is excited, a Gaussian THz pulse with central frequency ω_T,

$$E_{\text{THz}}(\omega_T,t,\phi) = F_T\exp\left[-\left(\frac{t-t_0}{\tau_T}\right)^2\right]\cos[\omega_T(t-t_0)+\phi], \quad (10)$$

may be amplified in the system. In Eq. (10), τ_T is the length of the THz pulse and F_T is the amplitude of the pulse. The average linear THz susceptibility for the THz pulse is given by

$$\chi(\omega_T) = N\int[\langle P_{\text{intra}}^{\omega_T}(\omega,0)\rangle - \langle P_{\text{intra}}^{\omega_T}(\omega,\pi)\rangle]d\omega, \quad (11)$$

where $N^{-1}\equiv 2\varepsilon_0\int E_{\text{THz}}^{\omega_T}(\omega,0)d\omega$ and $E_{\text{THz}}^{\omega_T}(\omega,\phi)$ and $\langle P_{\text{intra}}^{\omega_T}(\omega,\phi)\rangle$ are the Fourier transforms of the THz pulse and intraband polarization, respectively. The subtraction procedure is used to remove the dc component and the second-order nonlinear susceptibility from the response. The integration over ω gives the average susceptibility at frequency ω_T, which is the appropriate quantity when considering the gain of the THz pulse as a whole. The average gain coefficient $\gamma(\omega_T)$ and the refractive index $n(\omega_T)$ can be obtained numerically using

$$n - i\frac{\gamma(\omega_T)c}{2\omega_T} = \sqrt{\epsilon_s + \chi(\omega_T)},$$

where c is the speed of light in vacuum and $\epsilon_s=12.5$ is the static dielectric function of the unexcited BSSL. Thus, the gain coefficient is given explicitly by

$$\gamma(\omega_T) = -2\omega_T\,\text{Im}\{\sqrt{\epsilon_s+\chi(\omega_T)}\}/c. \quad (12)$$

III. NUMERICAL RESULTS AND DISCUSSION

In this section, we present the results of calculations of the intraband polarization and THz gain coefficients. We show that large THz gain persists over a large range of bias fields, which allows for a large range of tuning of the THz gain. We also discuss the influence of the HIES on the gain coefficients.

A. Intraband polarization

The BSSL is excited by a Gaussian optical pulse,

$$E_{\text{opt}}(t) = E_0\cos(\omega_c t)\exp[-(t/\tau)^2],$$

where E_0 is the pulse amplitude and the central frequency ω_c is set to be in resonance with $n=0$ 1*s* heavy-hole excitonic state at the given field. The optical pulse width τ is taken to be 590 fs. Because the optical pulse spectral width [full width at half maximum (FWHM)=0.9 THz (3.7 meV)] is much less than ω_B (for $F_o=15$ kV/cm, $\nu_B=3.0$ THz), the only 1*s* excitonic state that is optically excited is the $n=0$ state (see Fig. 2) and we do not form a Bloch-oscillating wave packet in the absence of a THz pulse. With this choice of central frequency, because the $n=0$ 1*s* state energy changes by less than 3 meV for $15\text{ kV/cm}<F_o<60\text{ kV/cm}$ (see Fig. 1), one need not change ω_c when the bias field is changed and can simply fix the pulse center at $\hbar\omega_c=1585.6$ meV. However, to simplify our discussion of the field dependence of the gain, we do adjust ω_c with the field. In all simulations, we also adjust E_0 such that the total areal carrier density after the pulse has passed is always $\rho=0.8\times10^9/\text{cm}^2$. This density is chosen to be low enough so as to avoid nonlinear effects such as exciton-exciton effects, dynamic screening, and phase-space filling discussed earlier.[19] If such effects are not present or are minimal, then the THz gain coefficients will simply scale linearly with the

carrier density (or optical intensity). Thus, it will certainly be possible to obtain higher gain coefficients than are calculated here, but they may be affected somewhat by many-body effects.

The THz pulse that is to be amplified is the Gaussian pulse given in Eq. (10), where we take $\tau_T=820$ fs and we consider a wide range of ω_T. Except in Sec. IV, where we address the issue of gain saturation, we take the pulse amplitude to be $F_T=0.3$ kV/cm. For this amplitude, we find that THz gain saturation is negligible.[13]

In all calculations, we use interband and intraband dephasing times of $T_{2\text{inter}}=1.0$ ps and $T_{2\text{intra}}=1.5$ ps, respectively. These values follow the relation $T_{2\text{intra}}\approx 1.5T_{2\text{inter}}$ that has been shown experimentally[25] and theoretically[17] in BSSLs. Since the exciton decay time is expected to be much longer than dephasing time, we choose it to be $T_1=5$ ps. The population decay time, which is determined by intraexcitonic scattering, has relatively little effect on the results as long as it is greater than $T_{2\text{intra}}$. The results also depend only very weakly on the *interband* dephasing time as long as the optical pulse intensity is adjusted to produce the same total carrier density. For example, when we reduce $T_{2\text{inter}}$ to 0.25 ps, the gain spectral shape is essentially unchanged and the peak gain is only reduced by approximately 10%. This indicates that apart from its effect on the total carrier density created for a given pulse, the interband coherence plays almost no role in the THz gain. Consequently, the THz pulse does not have to overlap with the optical pulse; the only requirement is that the THz pulse must arrive before exciton population has decayed substantially. The dependence on the *intraband* dephasing time $T_{2\text{intra}}$ is much stronger than the dependence on $T_{2\text{inter}}$. The gain spectra are qualitatively the same for $0.3\text{ ps}<T_{2\text{intra}}<2$ ps. However, for a fixed carrier density, the peak THz gain increases by approximately a factor of 2 as $T_{2\text{intra}}$ changes from 0.3 to 2.0 ps.

We consider pulsed operation so as to simplify the computations and to reduce the sensitivity of the results to the details of the particular dephasing and population decay models employed; we expect qualitatively similar results for longer pulses, but such long-time simulations require more sophisticated models of scattering and carrier extraction at the BSSL boundaries that are beyond the scope of the present paper and depend on the details of the BSSL biasing structure.

The intraband polarization calculated using the $1s$ and full bases is plotted in Fig. 3 for $F_o=15$ kV/cm for three different ω_T. Figure 3(a) shows the intraband polarization with an external THz field that is well off resonance with the excitonic transitions. The quasi-dc contribution to the polarization is due to the permanent intraband dipole moments of the excitonic states excited by the pulse. There are no large BOs evident for two reasons. First, the optical pulse only excites a significant population in $n=0$ state so that no coherent superposition state is created that can give rise to BO. Second, the external THz field used is not resonant with any transitions between WSL state; thus, it cannot significantly couple excitonic WSL levels. However, for an external THz field that is resonant with some transitions between excitonic, WSL states, the BO can be clearly seen in the intraband polarization [Figs. 3(b) and 3(c)].

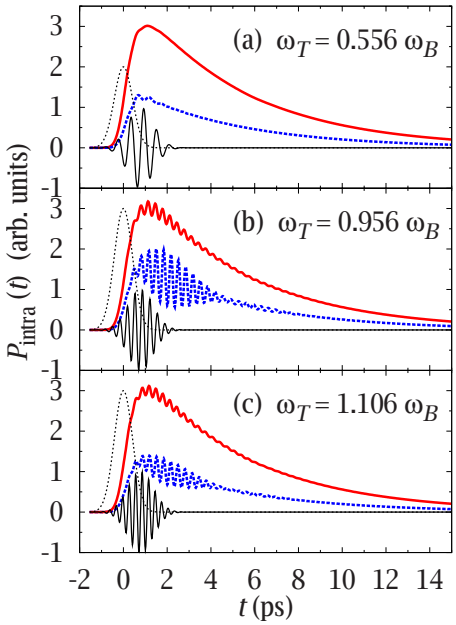

FIG. 3. (Color online) Temporal evolution of the intraband polarization calculated using the $1s$ (dashed blue line) and full (solid red line) bases for $F_o=15$ kV/cm. The profile of the optical pulse (dotted black line) and THz pulse (thin black line) is also shown.

In Fig. 3(b), we have $\omega_T=0.956\omega_B=\omega_{0,-1}$, where $\omega_{n,m}\equiv\omega_n-\omega_m$. The incident THz field frequency has been chosen so as to resonantly couple the $n=0$ and $n=-1$ $1s$ states. As a result, $1s$ excitons in the $n=0$ state are coherently driven down to the $n=-1,1s$ state by the THz pulse. Because $\omega_{+1,0}=1.041\omega_B$, the $n=0$ to $n=+1$ transition is not excited by the THz pulse and the carriers are only driven *down* the WSL. This *stimulated emission* process amplifies incident THz pulse as is indicated by the relative phases of the oscillations in the polarization and incident THz field. The full-basis result has lower-amplitude BOs than the $1s$ result (for the same total carrier density) because for $F_o=15$ kV/cm, almost half of the carriers excited by the optical pulse are not $n=0$ $1s$ excitons but are HIESs with $n<0$ [see Fig. 2(a) and earlier discussion].

For comparison purposes, in Fig. 3(c), we plot the intraband polarization for $\omega_T=1.106\omega_B$ where absorption of the external THz pulse is expected because ω_T is close to the transition between $n=0$ and $n=1$ excitonic states. Similar to Fig. 3(b), large amplitude BOs are also seen in the intraband polarization due to the coupling of two excitonic states. However, the relative phase between the external THz pulse and the intraband polarization in Fig. 3(c) differs from that in Fig. 3(b) by roughly π. Thus, while in the case of Fig. 3(b) work is being done by the excitons on the field and the field experiences gain, in the case of Fig. 3(c), work is done by the field on the excitons and the field experiences loss.

B. Gain coefficients

In Fig. 4, we present the gain spectra calculated using the two different bases for bias fields of $F_o=15$, 30, and 60 kV/cm. As can be seen, for each bias field, there is a

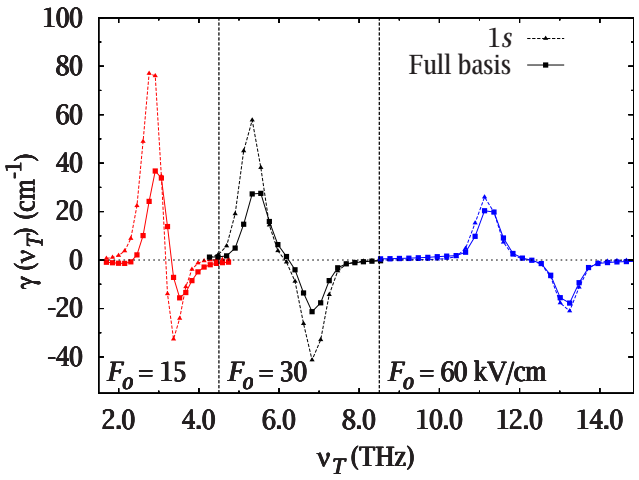

FIG. 4. (Color online) The THz gain spectra calculated using the full (solid line with squares) and 1*s* (dashed line with triangles) bases for three different dc bias fields.

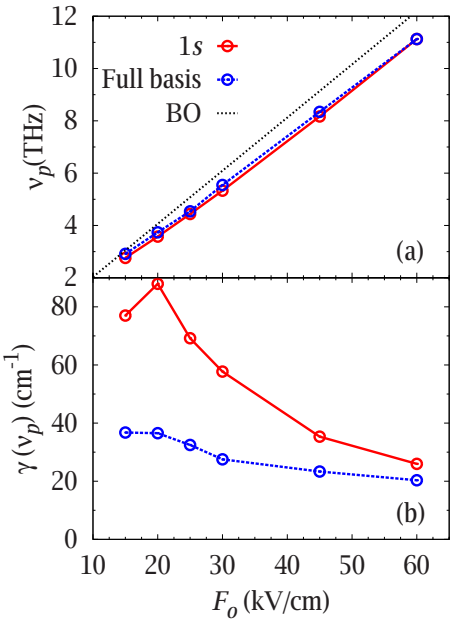

FIG. 5. (Color online) (a) The peak gain frequency ν_p and the BO frequency ν_B (black dotted line) as a function of the bias field F_o. (b) The peak gain $\gamma(\nu_p)$ as a function of bias field F_o. The results for both the 1*s* basis (solid red) and full basis (dashed blue) are shown on both plots.

frequency region of gain and a frequency region of loss. When $\omega_T \simeq \omega_{0,-1}$, there is gain, while when $\omega_T \simeq \omega_{+1,0}$, there is loss. Because at all bias fields $\omega_{0,-1} < \omega_B$ and $\omega_{+1,0} > \omega_B$, then roughly speaking, there is gain for $\omega_T \lesssim \omega_B$ (thus, $\nu_p < \nu_B$) and absorption for $\omega_T \gtrsim \omega_B$. The maximum gain is larger than the maximum loss because, due to excitonic effects, the intraband dipole matrix element is larger for the hh_0 to hh_{-1} transition than for the hh_0 to hh_{+1} transition. The width of the gain peaks is largely determined by the spectral width of the THz pulse (FHWM=0.65 THz).

We see from Fig. 4 that at lower bias fields, the gain is significantly reduced from the 1*s* result when the full basis (including HIES) is employed. This is primarily because the 1*s* states only make up a fraction of the excitons created by the optical pulse at such bias fields. Since the gain is largely coming from the 1*s* states (due to the large asymmetry in the 1*s* exciton WSL spacing), the net gain is reduced relative to that calculated using a pure 1*s* basis. This is clearly seen by comparing the results at F_o=15 kV/cm with those at F_o =60 kV/cm. For F_o=15 kV/cm, as can be seen from Fig. 1(a), almost half of the absorption at the optical pulse frequency is arising from $n=-1$ and $n=-2$ HIESs and the gain is accordingly reduced by approximately a factor of 2. In contrast, for F_o=60 kV/cm, almost all of the absorption is due to the creation of 1*s* excitons [see Fig. 2(b)] and the gain found using the two different bases is almost the same. Thus, we see that the effect of including HIES on the gain is relatively modest, with at most a decrease by a factor of 2 for a given total carrier density.

In Fig. 5, we plot the peak gain frequency ν_p and the peak gain coefficient $\gamma(\nu_p)$ as a function of the bias field. As can be seen, the peak gain frequency is always slightly smaller than the Bloch frequency ν_B due to excitonic effects. Also, the gain coefficient is greater than 20 cm^{-1} over the full range of dc bias fields considered. Thus, the system exhibits high gain over a tuning range of 3–11 THz. Although gain can be achieved at slightly lower bias fields than 15 kV/cm (and hence lower THz frequencies), we are limited by the fact that the $n=0$ excitonic peak loses its optical oscillator strength at a field of 9 kV/cm (see Fig. 1) and that at this same field the excitonic binding energy becomes comparable to $\hbar\omega_B$ and the excitonic WSL is effectively destroyed. Significant gain can also be achieved at bias fields above 60 kV/cm. However, as can be seen (Fig. 5), for the 1*s* basis the gain coefficient decreases approximately as $1/F_o$ for large F_o due to Wannier-Stark-localization-induced decrease in the intraband transition dipole matrix elements between neighboring WSL states.[15] At higher fields still, Zener tunneling destroys the WSL and the gain.

IV. COHERENT CASCADING EFFECTS ON GAIN SATURATION

In this section, we examine gain saturation in the BSSL system by considering the peak gain coefficient as a function of the amplitude of the THz field. By comparing our results to those of a comparable two-level excitonic system, we show that the gain saturates much more slowly in a BSSL than in a comparable two-level system. To explain this difference, in Sec. IV B, we present the results for an analytical model of a multilevel cascading system, with equal level spacings, and show that it exhibits similar gain saturation characteristics to our BSSL. The advantage of the multilevel cascading BSSL essentially arises from the fact that one exciton can result in the stimulated emission of many THz photons, thus reducing the degree of gain saturation. This effect can increase the gain saturation intensity by up to a factor of 4, but more importantly, it can lead to enhancement factors for large THz fields of up to $(N-1)/2$, where N is the number of periods in the BSSL.

A. Gain saturation in the biased semiconductor superlattice

When the THz field is approximately resonant with the $n=0$ to $n=-1$ transition, it is far from resonance with the $n=0$ to $n=+1$ transition. Thus, there is essentially no THz absorption due to the $n=0$ to $n=+1$ transition when $\omega_T=\omega_{0,-1}$, which is the frequency of peak gain. Therefore, the $n=0$ is effectively the upper state of the WSL when we are in this resonant condition. Although, for this frequency, the THz field is not exactly in resonance with the lower transitions (e.g., $n=-1$ to $n=-2$), it is much closer to resonance for these transitions (which have transition frequencies less than ω_B, see Table I) than to the $n=0$ to $n=+1$ transition. For short, low-amplitude THz pulses, the $n=0$ to $n=-1$ transition dominates the response. As the THz field amplitude is increased, the carriers will be *coherently driven* by the THz field down to the lower levels, resulting in considerable additional gain arising from transitions between lower levels.

There are two important effects associated with the coherent cascading. First, because the lower levels are constantly being coherently depopulated, the BSSL does not suffer the inversion-saturation problem that a two-level coupled quantum well (CQW) system would. This issue of buildup of carrier populations is important in such structures, and much effort has been spent in dealing with this problem in the design of QCLs. To operate our BSSL in steady state, we would still have to sweep the carriers out of the lowest WSL level, similar to what is done in a QCL, but for pulsed operation, this is not a significant constraint, as it has been shown that carrier sweep-out will occur on a time scale of roughly 10 ps for a system similar to ours.[18]

The second important effect of cascading is that the BSSL gain saturates much more slowly than in a two-level CQW due to the fact that one carrier (exciton) can be stimulated to make many transitions down the WSL, emitting one THz photon with each transition. This cascading process is similar to that exploited in a QCL except that rather than relying on phonon relaxation to connect different levels (as in a QCL), the process is coherent.

To demonstrate the effects of the coherent cascading on gain saturation, in Fig. 6, we present the THz gain coefficient as a function of the square of the THz field amplitude for $F_o=30$ kV/cm at the THz frequency of maximum small-signal gain, $\omega_T=0.875\omega_B$. We present the results for both the $1s$ basis and the full basis. As can be seen, the gain saturation is similar for both models but is somewhat reduced in the full-basis model due to the presence of HIES. For comparison, we also present the results for a *modified* $1s$ basis BSSL, where we remove the cascading effect by including only the $n=0$ and $n=-1$ states, thereby creating a simplified two-level (TL) system. As can be seen, although at very low THz field amplitudes the gain for the BSSL with the $1s$ basis is identical to that of the TL system, the gain is considerably larger in the BSSL relative to the TL for large field amplitudes. If we define the saturation field to be the field at which the gain coefficient decreases to half its small-signal value, then we see that for the BSSL, the saturation field is $F_{\mathrm{sat}}^{\mathrm{BSSL}}\simeq 5.3$ kV/cm, while for the TL system, it is $F_{\mathrm{sat}}^{\mathrm{BSSL}}\simeq 4.4$ kV/cm. Thus, the saturation field is roughly a factor of 1.2 higher for the BSSL than for an equivalent two-level model. Although this is a modest increase, the increase in the high-field gain is much more substantial. For example, the BSSL gain is roughly six times larger than the TL model gain for $F_T=10$ kV/cm.

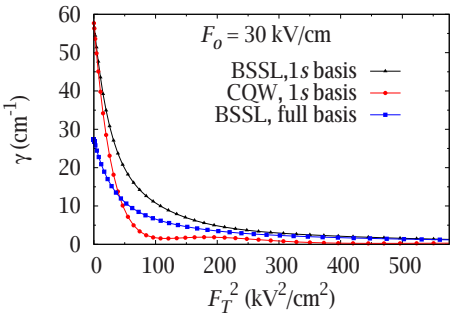

FIG. 6. (Color online) THz gain as a function of the square of the applied THz field amplitude for $F_o=30$ kV/cm at THz frequency of $\omega_T=0.875\omega_B$. The THz frequency is chosen to be resonant with $n=0$ to $n=-1$ transition.

The cascading effect is even greater if we detune our field such that it is closer to the resonance frequencies between the lower WSL levels, so as to favor the transitions between lower excitonic states (see Table I). In Fig. 7, we plot the same quantities as in Fig. 6 but now for a THz frequency of $\omega_T=0.95\omega_B$. Comparing to the results in Fig. 6, we see that the small-signal gain is reduced significantly. However, the saturation of the gain is much less for the BSSL for this THz field. For the BSSL with the $1s$ basis, the saturation field is $F_{\mathrm{sat}}^{\mathrm{BSSL}}\simeq 13.9$ kV/cm, while for the TL system, it is $F_{\mathrm{sat}}^{\mathrm{BSSL}}\simeq 4.3$ kV/cm. Thus, the saturation field is roughly a factor of 3.2 higher for the BSSL than for an equivalent two-level model. For high fields, the gain in the BSSL can be as much as 30 times higher. This decrease in saturation in the BSSL is mainly caused by the faster cascading down of the BSSL when the frequency of the THz field is tuned closer to lower energy levels.

B. Simple model of biased semiconductor superlattice multilevel system

To better understand the gain saturation characteristics of the BSSL, in this section, we consider a simplified model.

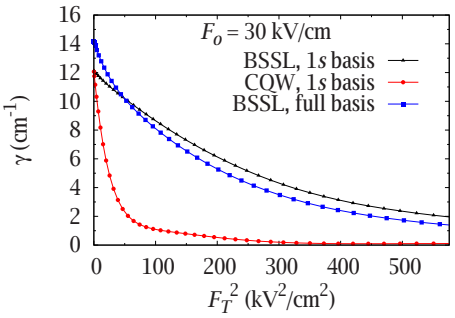

FIG. 7. (Color online) THz gain as a function of the square of the applied THz field amplitude for $F_o=30$ kV/cm at THz frequency of $\omega_T=0.95\omega_B$. The THz frequency is chosen to be in closer resonance with the lower-level transitions than the frequency used in Fig. 6.

We take the system to be represented by M equally spaced levels with energies given by $E_n = E_0 + n\hbar\omega_T$, where $n = \{0, -1, \ldots, -(M-1)\}$, E_0 is the energy of the top level, and $\hbar\omega_T$ is the energy difference between two neighboring energy levels, which is equal to the energy of the photons in the THz field. This is an idealization of our system, but it contains the two key ingredients: an upper energy level and many (roughly) equally spaced lower levels. To simplify the model further, we consider the THz field to be cw and assume that the carriers are being injected (by the optical field) into the $n=0$ level at a rate R_0. We can then consider the steady-state gain coefficient by determining the steady-state population distribution in the levels.

We follow the standard rate-equation approach[26] where, for simplicity, we neglect scattering between the levels but include a single time constant τ which accounts for scattering out of all levels. We include stimulated transitions through the stimulated emission rate W, where

$$W \equiv \frac{1}{2\tau}\left(\frac{F_T}{F_{\text{sat}}^{(2)}}\right)^2 \tag{13}$$

and $F_{\text{sat}}^{(2)}$ is the saturation THz field for a two-level system ($M=2$). This model neglects spontaneous emission for simplicity because we are only interested in the dependence of the high-field saturation effects on the number of levels. It is easy to show that the gain coefficient for our M-level system is given by

$$\gamma_M(W) = \gamma_M(0)\frac{[N_0(W) - N_{-(M-1)}(W)]}{[N_0(0) - N_{-(M-1)}(0)]}, \tag{14}$$

where $N_n(W)$ is the steady-state population in level n, when the stimulated rate is W, and $\gamma(0)$ is the small-signal gain, which can be shown to be independent of M.

We use the rate equations for the level populations and set $dN_n(W)/dt = 0$ to obtain steady-state equations:

$$\begin{pmatrix} -\left(W+\frac{1}{\tau}\right) & W & 0 & 0 & 0 \\ W & -\left(2W+\frac{1}{\tau}\right) & W & 0 & 0 \\ 0 & W & -\left(2W+\frac{1}{\tau}\right) & W & 0 \\ & & \ddots & & \\ 0 & 0 & 0 & W & -\left(W+\frac{1}{\tau}\right) \end{pmatrix} \begin{pmatrix} N_0 \\ N_{-1} \\ N_{-2} \\ \vdots \\ N_{-(M-1)} \end{pmatrix} = \begin{pmatrix} -R_0 \\ 0 \\ 0 \\ \vdots \\ 0 \end{pmatrix}. \tag{15}$$

This system of linear equations can be solved exactly[27] and yields the following solution:

$$\frac{N_0(W) - N_{-(M-1)}(W)}{R_0\tau} = \frac{(\alpha-1)(\alpha^M - \alpha)}{\alpha(\alpha^M + 1)}, \tag{16}$$

where α is a dimensionless quantity given by

$$\alpha = \frac{2W\tau}{2W\tau + 1 + \sqrt{4W\tau + 1}}. \tag{17}$$

Note that when $W=0$, then $\alpha=0$, and when $W\to\infty$, $\alpha \to 1$. With the exact solution of Eq. (16), we can now compare an M-level system to a two-level system. For the two-level system, from Eqs. (14) and (16), we obtain after some algebra

$$\gamma_2(W) = \frac{\gamma(0)}{1+2W\tau} = \frac{\gamma(0)}{1+(F_T/F_{\text{sat}}^{(2)})^2},$$

which is the standard, expected result. To see the results for different numbers of levels M, we plot the gain coefficients in Fig. 8 as a function of F_T^2. From this figure, we see that the gain saturation field increases as M is increased. If we define the saturation field $F_{\text{sat}}^{(M)}$ for the M-level system to be the field at which the gain coefficient is half of its small-signal value, then we find that for $M\to\infty$, $F_{\text{sat}}^{(M)} \to 2F_{\text{sat}}^{(2)}$. This limit is approached quite rapidly; for example, when $M=7$, $F_{\text{sat}}^{(M)} \simeq 1.94F_{\text{sat}}^{(2)}$. This result confirms the relative increase in the saturation field found in our BSSL simulations. More striking

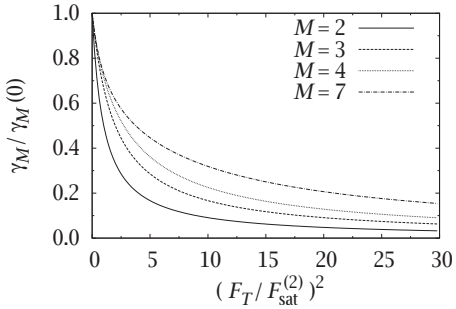

FIG. 8. Gain coefficient for our simplified M-level model of a BSSL as a function of the square of the applied THz field amplitude. The different curves are for the different numbers of levels used in the model.

than the increase in the saturation field is the increase in the gain coefficient at large F_T. It can be shown from Eqs. (14) and (16) that $\gamma_M(W)/\gamma_2(W)=M-1$ when $F_T \gg F_{\mathrm{sat}}^{(2)}$. This shows that the M-level system is much more robust to saturation than the two-level one. Based on this result, we can conclude that our BSSL system is acting roughly like a six-level system for the time constants and pulse durations that we have used. The fact that only six levels appear to be contributing is because our system is not operating in steady state and the levels are not exactly in resonance. Despite this, it is clear that coherent cascading is playing a significant role even in pulsed operation.

Finally, we briefly comment on the comparison of our coherent cascading system to a QCL. A simple model of a QCL consists of a set of two-level systems coupled together by phonon-induced scattering from the bottom level of one two-level system to the top level of the next. Using this model, we find that if the rate $1/\tau_1$ at which the phonons scatter the electrons to next stage is much faster than the THz field driving rate W, then for high fields ($W\tau \gg 1 \gg W\tau_1$), the QCL gain scales as $\gamma_M^{\mathrm{QCL}}(W)/\gamma_2^{\mathrm{QCL}}(W)=M-1$, just as in the case of the coherently driven system. However, if the THz field is sufficiently large such that the phonon scattering rate is less than the THz driving rate, i.e., $W\tau_1 \gg 1$ and $\tau_1 \lesssim \tau$, then the gain ratio saturates at the value $\gamma_M^{\mathrm{QCL}}(W)/\gamma_2^{\mathrm{QCL}}(W) = 1+\tau/(2\tau_1)$ for large M. This is because the field drives the carriers to lower levels faster than the phonon scattering can depopulate them. In contrast, in the coherently driven system, the THz field itself ensures that the carriers are driven to the lower levels even faster when the THz field amplitude is increased. Thus, it is expected that a coherently driven multilevel system could exhibit superior saturation characteristics to a QCL under certain conditions.

V. CONCLUSION

In summary, we have theoretically demonstrated large tunable THz gain in an undoped photoexcited semiconductor superlattice that is robust even when all continuum states are included in the calculation. This gain mechanism differs from the usual phonon-assisted gain mechanism proposed for BSSLs and is expected to be considerably larger for an undoped, optically excited BSSL. By adjusting the bias field, the gain is tunable over a range of 3–11 THz. We have also shown that due to coherent cascading of the carriers, the system has relatively high saturation fields and is much more robust to saturation than a comparable two-level system.

Although our calculations have only been performed for a 0.82 ps THz pulse, gain should be sustained for much longer pulses. The key requirement is that the carriers are swept out of the system fast enough such that they do not result in a depolarization field or loss of population inversion. Recent experiments in very similar BSSLs have demonstrated fast carrier sweep-out (~100 ps) even in the absence of coherent cascade.[18] Thus, with the coherent cascading effect in conjunction with phonon relaxation, it is fully expected that gain will be sustained for pulses much longer than 0.82 ps. Detailed verification of this requires a sophisticated treatment of long-time scattering and boundary effects and is the topic of future work.

ACKNOWLEDGMENTS

This work was supported in part by the Natural Sciences and Engineering Research Council of Canada. We acknowledge the use of the HPCVL computing facility.

[1] J. Faist, F. Capasso, D. L. Sivco, C. Sirtori, A. L. Hutchinson, and A. Y. Cho, Science **264**, 553 (1994).
[2] R. Kohler, A. Tredicucci, F. Beltram, H. E. Beere, E. H. Linfield, A. G. Davies, D. A. Ritchie, R. C. Iotti, and F. Rossi, Nature (London) **417**, 156 (2002).
[3] A. Tsekoun, R. Go, M. Pushkarsky, M. Razeghi, and C. K. N. Patel, Proc. Natl. Acad. Sci. U.S.A. **103**, 4831 (2006).
[4] J. A. Fan, M. A. Belkin, F. Capasso, S. Khanna, M. Lachab, A. G. Davies, and E. H. Linfield, Opt. Express **14**, 11672 (2006).
[5] J. Xu, J. M. Hensley, D. B. Fenner, R. P. Green, L. Mahler, A. Tredicucci, M. G. Allen, F. Beltram, H. E. Beere, and D. A. Ritchie, Appl. Phys. Lett. **91**, 121104 (2007).
[6] B. G. Lee, M. A. Belkin, R. Audet, J. MacArthur, L. Diehl, C. Pflugl, F. Capasso, D. C. Oakley, D. Chapman, A. Napoleone, D. Bour, S. Corzine, G. Hofler, and J. Faist, Appl. Phys. Lett. **91**, 231101 (2007).
[7] G. H. Wannier, Phys. Rev. **117**, 432 (1960).
[8] R. Ferreira and G. Bastard, Surf. Sci. **229**, 424 (1990).
[9] A. A. Ignatov, K. F. Renk, and E. P. Dodin, Phys. Rev. Lett. **70**, 1996 (1993).
[10] Y. A. Tarakanov, M. A. Odnoblyudov, K. A. Chao, N. Sekine, and K. Hirakawa, Phys. Rev. B **74**, 125321 (2006).
[11] M. M. Dignam and J. E. Sipe, Phys. Rev. Lett. **64**, 1797 (1990).
[12] J. M. Lachaine, M. Hawton, J. E. Sipe, and M. M. Dignam, Phys. Rev. B **62**, R4829 (2000).
[13] A. Zhang, D. Wang, and M. M. Dignam, Appl. Phys. Lett. **86**, 171110 (2005).
[14] C. P. Holfeld, F. Loser, M. Sudzius, K. Leo, D. M. Whittaker, and K. Kohler, Phys. Rev. Lett. **81**, 874 (1998).
[15] L. Yang, B. Rosam, J.-M. Lachaine, K. Leo, and M. M. Dignam, Phys. Rev. B **69**, 165310 (2004).
[16] M. Hawton and M. M. Dignam, Phys. Rev. Lett. **91**, 267402 (2003).
[17] A. Zhang and M. M. Dignam, Phys. Rev. B **69**, 125314 (2004).
[18] A. Lisauskas, C. Bloser, R. Sachs, H. G. Roskos, A. Juozapavicius, G. Valusis, and K. Kohler, Appl. Phys. Lett. **86**, 102103 (2005).
[19] L. Yang, B. Rosam, and M. M. Dignam, Phys. Rev. B **72**, 115313 (2005).
[20] M. M. Dignam and J. E. Sipe, Phys. Rev. B **43**, 4097 (1991).
[21] M. M. Dignam and J. E. Sipe, Phys. Rev. Lett. **64**, 1797 (1990).
[22] M. M. Dignam and M. Hawton, Phys. Rev. B **67**, 035329 (2003).
[23] D. Wang, M. Hawton, and M. M. Dignam, Phys. Rev. B **76**, 115311 (2007).

[24] V. M. Axt, G. Bartels, and A. Stahl, Phys. Rev. Lett. **76**, 2543 (1996).
[25] P. H. Bolivar, F. Wolter, A. Müller, H. G. Roskos, H. Kurz, and K. Köhler, Phys. Rev. Lett. **78**, 2232 (1997).
[26] C. C. Davis, *Lasers and Electro-Optics: Fundamentals and Engineering* (Cambridge University Press, Cambridge, 1996).
[27] H. A. Yamani and M. S. Abdelmonem, J. Phys. A **30**, 2889 (1997).